JOURNAL OF CHEMICAL INFORMATION AND MODELING

Article

pubs.acs.org/jcim

Virtual Screening Yields Inhibitors of Novel Antifungal Drug Target, Benzoate 4-Monooxygenase

Sabina Berne,*[,†,∥] Barbara Podobnik,[‡,∥] Neja Zupanec,[§] Metka Novak,[§] Nada Kraševec,[§] Samo Turk,[⊥] Branka Korošec,[§] Ljerka Lah,[§] Erika Šuligoj,[§] Jure Stojan,[†] Stanislav Gobec,[⊥] and Radovan Komel*[,†,§]

[†]Faculty of Medicine, Institute of Biochemistry, University of Ljubljana, Vrazov trg 2, SI-1000 Ljubljana, Slovenia

[‡]Lek Pharmaceuticals d.d., Verovškova 57, SI-1000 Ljubljana, Slovenia

[§]Laboratory for Molecular Biology and Nanobiotechnology, National Institute of Chemistry, Hajdrihova 19, SI-1000 Ljubljana, Slovenia

[⊥]Faculty of Pharmacy, Chair of Pharmaceutical Chemistry, University of Ljubljana, Aškerčeva cesta 7, SI-1000 Ljubljana, Slovenia

Supporting Information

ABSTRACT: Fungal CYP53 enzymes are highly conserved proteins, involved in phenolic detoxification, and have no homologues in higher eukaryotes, rendering them favorable drug targets. Aiming to discover novel CYP53 inhibitors, we employed two parallel virtual screening protocols and evaluated highest scoring hit compounds by analyzing the spectral binding interactions, by surveying the antifungal activity, and assessing the inhibition of catalytic activity. On the basis of combined results, we selected 3-methyl-4-(1H-pyrrol-1-yl)benzoic acid (compound **2**) as the best candidate for hit-to-lead follow-up in the antifungal drug discovery process.

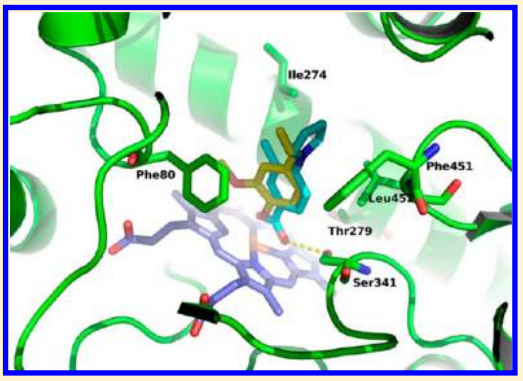

INTRODUCTION

The incidence of invasive fungal infections (IFI) is increasing, particularly among immunocompromised patients, like individuals infected with HIV, transplant recipients, and patients with cancer.[1−3] Although *Aspergillus* spp. and *Candida* spp. cause most of IFI, other molds such as *Fusarium* spp., dematiaceous fungi, and Mucorales (Zygomycota) have emerged as significant opportunistic pathogens in recent years.[4,5] Despite the introduction of new, more powerful antifungal agents, mortality due to fungal infections continues to be substantial.[3,6]

One of the leading business intelligence providers (GBI Research) has evaluated the global antifungals market at $9.4 billion in 2010 with a compound annual growth rate of 2.9% from 2002 to 2010.[7] Furthermore, their analysis has shown that the antifungals market is dominated by generics with only 38 molecules in Research and Development (R&D). Apart from the fungal cell wall, fungi are metabolically similar to mammalian cells and therefore offer few pathogen-specific targets, making antifungal drug R&D challenging. Present treatments rely on antifungals such as azoles that inhibit ergosterol biosynthesis, polyene antibiotics (amphotericin B), which disrupt the fungal cell membrane via channel formation, echinocandins (caspofungin, anidulafungin, micafungin) that inhibit glucan β1,3-synthase, the enzyme required for cell wall synthesis, and nucleoside analogs (5-fluorocytosine) that obstruct DNA and RNA synthesis.[8−11]

Fungal cytochromes P450 (CYPs) are a numerous and versatile group of highly specific enzymes with a pivotal role in xenobiotic detoxification. Fungal lanosterol 14α-demethylase, CYP51, has been selected as a prominent target for a wide array of effective azole inhibitors, with fluconazole, itraconazole, and voriconazole as major players in the rapidly expanding systemic antifungal market.[10,12,13] Unfortunately, azoles not only affect fungal CYP51 but also interfere with some mammalian xenobiotic-metabolizing CYPs (especially from families 1−3).[14,15] This leads to a range of unwanted drug interactions and results in adverse side effects and toxicity.[16,17]

Fungal CYPs with high substrate specificities and no homologues in mammalian genomes are therefore promising novel therapeutic targets. Enzymes of the CYP53 family (EC 1.14.13.12) are highly conserved proteins (Figure 1; protein alignment with characteristic structural features is available in Figure S1, Supporting Information) widely distributed in fungi, including the pathogenic *Aspergillus fumigatus* and *Gibberella zeae*. They catalyze para-hydroxylation of benzoic acid, its derivatives, and other naturally occurring phenolic plant defense compounds.

In our preceding study,[19] we identified benzoate 4-monooxygenase (CYP53A15; benzoate para-hydroxylase; BPH) of the fungal pathogen *Cochliobolus lunatus* as a crucial

Received: September 18, 2012
Published: October 24, 2012

dx.doi.org/10.1021/ci3004418 | *J. Chem. Inf. Model.* 2012, 52, 3053−3063

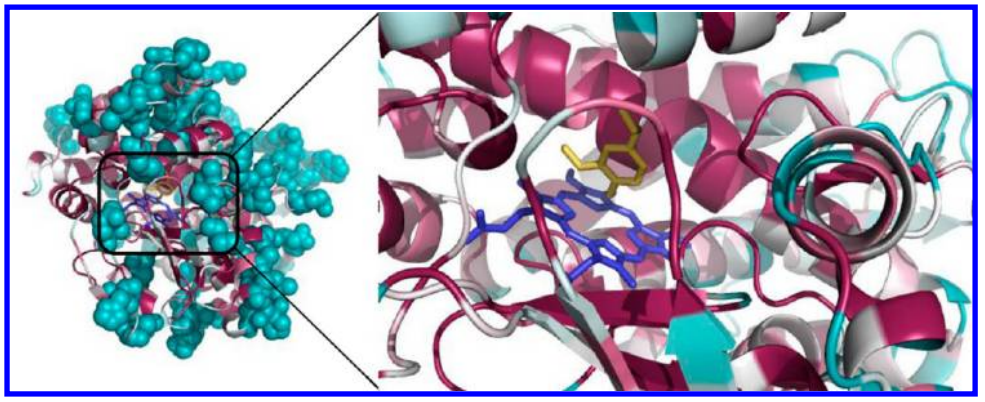

Figure 1. Conserved amino acid residues in the CYP53 protein model with a close-up of the enzyme active site as estimated by ConSurf.[18] The heme moiety is colored blue, ligand is yellow, identical residues are purple, and nonconserved residues are cyan.

enzyme involved in detoxification of benzoic acid (BA), a key intermediate in metabolism of aromatic compounds in fungi. We have also demonstrated that CYP53A15 activity was inhibited with natural phenolic compounds, such as isoeugenol, and revealed their antifungal potential.

In this work, we focused our research on the discovery of novel specific antifungal compounds by exploring the chemical properties of isoeugenol for ligand-based similarity searching, and using the CYP53A15 homology model for structure-based virtual screening. We analyzed forty highest scoring compounds in spectral binding titrations with CYP53A15, evaluated them as inhibitors of benzoate 4-monooxygenase, and assayed them for antifungal activity. On the basis of its potent antifungal activity and good inhibition of CYP53A15 enzyme activity, we selected 3-methyl-4-(1*H*-pyrrol-1-yl)benzoic acid (compound **2**) as a candidate for hit-to-lead follow-up in the antifungal drug discovery process.

EXPERIMENTAL SECTION

Virtual Screening of the Compound Library and Molecular Docking into the CYP53A15 Active Site. *Computer Hardware.* We carried out all computations on two workstations. The first workstation had four dual core AMD Opteron 2.0 GHz processors, 16 GB RAM, four 320 GB hard drives in a RAID10 array, and Nvidia GeForce 7900 graphic cards; this workstation was running the 64-bit Fedora 7. The second workstation had two quad core Intel Xeon 2.2 GHz processors, 8 GB RAM, 320 GB and 1TB hard drives, and a Nvidia Quadro FX 4800 graphic card and was running the current version of the 64-bit Arch Linux.

Compound Database Preparation. We selected compound 3D structures from the U.S. National Cancer Institute (NCI) Bank of Compounds (http://www.dtp.nci.nih.gov), the Asinex Library of Compounds (Asinex, Moscow, Russia; http://www.asinex.com/Libraries.html), ChemBridge (ChemBridge, San Diego CA; http://www.chembridge.com/screening_libraries), and Maybridge Screening Collections (Maybridge, Cornwall, England; http://www.maybridge.com), and downloaded them from the ZINC database[20] to construct a diverse chemical library of 1.8 million compounds. We generated a more focused compound library of manageable size with the FILTER application (Openeye Scientific Software, Inc.) and the following descriptors: molecular weight, 100−300 g/mol; number of ring systems, 1−3; number of heteroatoms, at least 2; number of H-bond donors, 0−4; number of H-bond acceptors, 0−6; and logP between −3.0 and 3.0. We used additional filtering parameters to eliminate compounds with reactive functional groups and to remove known aggregators (a function developed by Shoichet[21]). The resulting focused library consisted of roughly 143 000 structures.

Molecular Docking. We performed molecular docking on our previously reported[19] homology-built model of CYP53A15 (PMDB ID: PM0075149) from *Cochliobolus lunatus* using FlexX 3.1 (BioSolveIT GmbH).[22] We defined the docking active site as the volume of the enzyme within 5.5 Å of the isoeugenol ligand in the homology-built model. Prior to docking, we assigned protonation states and orientation of amino acid residues within the enzyme active site manually, to fulfill constraints imposed by the binding site. Octahedral coordination was assigned to the heme iron (Fe^{2+}). We instructed the docking program to consider only those solutions that predict interactions with the heme iron within the enzyme active site. For the base placement, we used Triangle Matching: this program generated the maxima of 200 solutions per iteration and 200 per fragmentation. We validated the system with isoeugenol by a docking run with the above-mentioned settings. Finally, we docked all of the 143 000 compounds into the enzyme active site using the same parameters as for the validation run. We ranked the compounds according to the best scored conformation. Thirty-two of those compounds were available and subsequently evaluated in in vitro experiments.

Similarity Search. Parallel to the docking experiment, we performed a similarity search using FTrees 2.3 (BioSolveIT GmbH).[23] Isoeugenol was used as a query. The program used the Dynamic Match-Search algorithm, and the Subgraph weight was set to 0.5. Finally, we searched the 143 000-compound database for compounds with similar structural features as isoeugenol. From the compounds with highest similarity to isoeugenol, we evaluated eight available compounds in vitro.

Compound Chemical Characterization. Among highest ranking hits from the VS process, forty compounds were selected and purchased from the ChemBridge (see Chart S1, Supporting Information, for their structures and scores). We assessed the purity of active hit compounds **1**−**10**, **12**, **23**, and **24** using reversed-phase high-performance liquid chromatography (HPLC) analysis on an Agilent 1100 system (Agilent Technologies, Santa Clara, CA, USA) equipped with a quaternary pump and a multiple-wavelength detector, using an Agilent Eclipse Plus C18, 5 μm (150 × 4.6 mm) column. We dissolved the compounds in 40% acetonitrile/water at 0.16 mg/mL final concentration and injected 10 μL onto the column.

dx.doi.org/10.1021/ci3004418 | *J. Chem. Inf. Model.* 2012, 52, 3053−3063

We used acetonitrile as an organic modifier and 0.1% trifluoroacetic acid in water as an aqueous buffer. The elution was performed with a 1.0 mL/min flow rate using a linear gradient from 25% to 70% acetonitrile over 15 min, followed by 4 min at 70% acetonitrile, then back down to 25% acetonitrile over 1 min, and followed by 7 min equilibration between samples. Detection was at 220 nm. The relative purity of all of the active compounds, except compound **3**, was above 95.0% as determined by HPLC.

^{1}H NMR spectra were recorded on a Bruker AVANCE III 400 MHz spectrometer in DMSO-d_6 solution, with tetramethylsilane as the internal standard. Mass spectra were obtained using a VG-Analytical Autospec Q mass spectrometer. Results of compound characterization are available in S2, Supporting Information.

Expression, Purification, and Enzymatic Activity of Recombinant CYP53A15 and CPR. We expressed *Cochliobolus lunatus* CYP53A15 as a C-terminally His_4-tagged protein in *E. coli* C43(DE3) cells and purified from bacterial membranes with Ni-NTA affinity chromatography as described previously.[24] The eluted protein was dialyzed against 20 mM Na-phosphate (pH 7.4)/0.5 M NaCl/20% glycerol/0.1 mM EDTA, aliquoted and stored at −80 °C.

We prepared *C. lunatus* cytochrome P450 reductase (CPR1) as a C-terminally His_6-tagged protein as reported in Lah et al.[24] Bacterial membranes harboring the recombinant CPR were resuspended in 50 mM K-phosphate (pH 7.4)/0.1 mM DTT/0.1 mM PMSF, aliquoted, and stored at −80 °C.

We assessed the total protein concentration using the Bradford method[25] and verified the purity of recombinant proteins with SDS-PAGE. We measured the enzymatic activity of the recombinant proteins as described in detail.[24]

Spectral Binding Titrations. The binding of substrate (BA) and hit compounds was investigated, following the divided cuvette method of Jefcoate.[26] To each cuvette, 1 mL of HGE (50 mM HEPES pH 7.4, 15% (v/v) glycerol, 0.1 mM EDTA) buffer was added to one chamber and 1 mL of protein sample (1.2 μM CYP53A15 in HGE buffer) to the other chamber. To obtain difference spectra, a baseline was recorded between 350 and 500 nm on a Perkin-Elmer LAMBDA 950 UV/vis/NIR spectrophotometer at 25 °C, followed by BA (20 μM−4 mM final concentration) or ligand titration (10−400 μM final concentration) to the protein sample in the sample cuvette and to the HGE buffer in the reference cuvette. Equilibration of samples upon adding the ligands was reached immediately after mixing, since no change in spectra could be detected in repeated scans. The final concentration of solvent (DMSO) was less than 1%. We normalized the absorbance data of difference spectra at the isosbestic point (407 nm). We plotted the changes in absorbance as a function of inhibitor concentration, at wavelengths selected on the basis of individual spectral characteristics. We estimated the spectral dissociation constants (K_s) and the magnitude of spectral binding ($\Delta A_{max}/K_s$) using nonlinear regression analysis to one site-specific binding equation with GraphPad Prism software (GraphPad Software, Inc., La Jolla, CA). Those parameters were used to describe affinities and potencies of compounds that interact with CYP53A15.

Fungal Growth Inhibition Assay. In a preliminary screening, we examined 33 soluble hit compounds for antifungal activity against the *Cochliobolus lunatus* strain MUCL 38696 (m118) (Friedrich Schiller University, Jena, Germany). Eight substances showing inhibitory effects were further evaluated. Briefly, MEA (Blakeslee's formula) agar plates were supplemented with inhibitor (0.5 mM final concentration of **1**, **3**, **5**, **7**; and 0.1 mM for **2**, **4**, **6**, and **8**), or solvent (DMSO) as control, and inoculated centrally with mycelial discs taken from 5-day-old fungal culture. We monitored mycelial growth daily at 28 °C. Experiments were performed in triplicates. We determined radial growth rates (RGR) from linear regression of best fit slope of growth curves and presented as a mean ± SE. Initial growth inhibition (IGI) was defined as the intercept on time axis where linear growth phase was extrapolated to a zero increase in diameter.[19]

CYP53A15 Inhibition Assay and Determination of K_i Values. *Reconstitution System.* We combined the purified CYP53A15 (1.1 μM) with membrane-bound CPR (29 μM) in HGE (50 mM HEPES pH 7.4, 15% (v/v) glycerol, 0.1 mM EDTA) buffer containing ergosterol (Erg)/sphingomyelin (SM)/1,2-dilauroylphosphatidylcholine (DLPC) (40:40:20 mol %) vesicles and dialyzed at +4 °C against HGE buffer for 2 h. Aliquots (500 μL) of reconstitution system (RS) were stored at −80 °C.

Inhibition of CYP53A15 Activity. In brief, a 400 μL reaction mixture containing 100 μL of RS, benzoic acid (BA; 50 μM final concentration), and varying concentrations of inhibitor (0, 20, 50, and 125 μM final concentration) was preincubated in HGE buffer (pH 7.4) at room temperature for 3 min, followed by addition of NADPH (1.1 mM final concentration) to start the reactions. After 5, 10, 25, 45, 90, 180, 300, and 420 min at room temperature, 60 μL of acetonitrile were injected into 40 μL of mixture to stop the reactions. We measured the CYP53A15 activity (using freshly prepared or stored RS as well as enzymes from different batches) in the absence and presence of inhibitors as described previously.[24] The exact starting concentrations of BA (ranging from 27.5 to 120 μM) were obtained by quantitative HPLC analysis, while CYP53A15 (0.7−1.1 μM) values were fitted to be within 10% of added enzyme concentration. From the time course curves of CYP53A15 mediated conversion of BA to 4-hydroxybenzoic acid in the presence or absence of inhibitors, we determined the K_i and K_M values using ENZO,[27] a web tool for easy construction and quick testing of kinetic models of enzyme catalyzed reactions. The results file can be accessed by loading ENZO project ID 120402501, selecting the "Set Parameters" tab and pressing "Start".

Molecular 3D Simulation. We carried out molecular 3D simulations for the CYP53A15-compound **2** complex in the active site channel. We obtained the CYP53A15 homology model[19] from the PMDB database.[28] For compound **2**, we searched atom types with the corresponding force field parameters in the CHARMM database[29] until we achieved good agreement between CHARMM and GAUSSIAN 03 (Gaussian, Inc.) optimized geometries (see the Supporting Information). Subsequently, we substituted the isoeugenol in CYP53A15 homology model with compound **2** by superimposing the aromatic rings of both molecules. For Fe^{2+} in heme, we applied the original parameters from the CHARMM force field file. After complex optimization, we ran 1 ns constant pressure and temperature (CPT) dynamic simulation (300 K, 1 bar, time step 1 fs) with the CHARMM molecular modeling program invoking the EWALD summation for calculating the electrostatic interactions. We used the final optimized structure as the end position in a dynamic simulation of compound **2** entering the active channel. We chose the command OVERLAP in CHARMM to conduct compound **2** from the outside to

that final position. We generated the visual simulation (see movie in the Supporting Information) by Visual Molecular Dynamics Software.[30]

RESULTS AND DISCUSSION

Virtual Screening. In recent years, virtual screening (VS) has become a complementary technology to high-throughput screening in probing for hit compounds in the pharmaceutical industry.[31−33] As the first step in the VS process, we narrowed down a composite chemical library of 1.8 million molecules with 3D structures obtained from commercial compound databases to a subset of roughly 143 000 compounds by a filtering procedure tailored under fragment-based rules.[34] After filtering, we applied two parallel VS approaches, a ligand-based similarity search and molecular docking. The complete filtering and screening process is depicted in Scheme 1.

Scheme 1. Overview of the VS Procedure in the Present Study

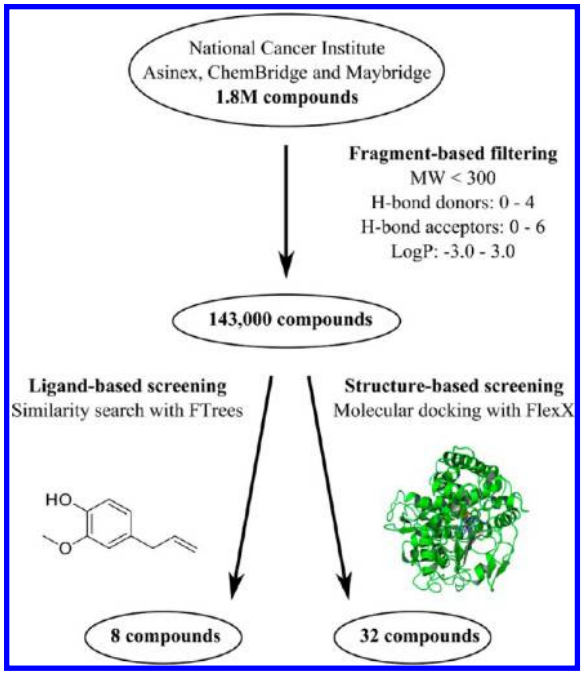

To explore chemical space around isoeugenol, identified as an inhibitor of CYP53A15 with antifungal properties in our previous studies,[19] we performed a ligand-based 2D similarity screening using Ftrees.[23] Eight compounds with the highest similarity to isoeugenol are listed in Chart S1 (Supporting Information). They were purchased and evaluated in vitro.

Since the crystal structure of CYP53A15 from *Cochliobolus lunatus* is unavailable, we used the homology-build model of CYP53A15[19] for molecular docking of the focused library of compounds with FlexX software.[22] Compounds were ranked according to the FlexX score. Available 32 top-ranked compounds (Chart S1, Supporting Information) were purchased and evaluated *in vitro*. As expected, molecular docking yielded structurally more diverse compounds than the ligand-based method.[35]

Due to their insolubility, we excluded seven compounds from further inspection (Chart S1, Supporting Information). Subsequently, we analyzed the remaining 33 compounds in spectral binding titration with CYP53A15 and investigated their antifungal potential in the fungal growth inhibition assay. We further tested eight compounds that exhibited antifungal activity for inhibition of CYP53A15 activity in reconstitution systems.

Spectral Binding Analysis of Hit Compounds with CYP53A15. The binding of a ligand to CYP elicits three types of spectral changes.[36] Type I ligands induce difference spectra with a broad peak in the region of 370−390 nm and a trough in the region of 400−450 nm, indicative of the change from a low- to high-spin state of the ferric iron. This shift in iron spin equilibrium is characteristic of substrate binding and is associated with the displacement of a water molecule bound to the heme iron, converting the iron coordination number from six to five.[37] As a typical substrate, BA induces the characteristic type I optical change upon binding to the CYP53A15 (Figure 2A). Spectra with a maximum at 386 nm,

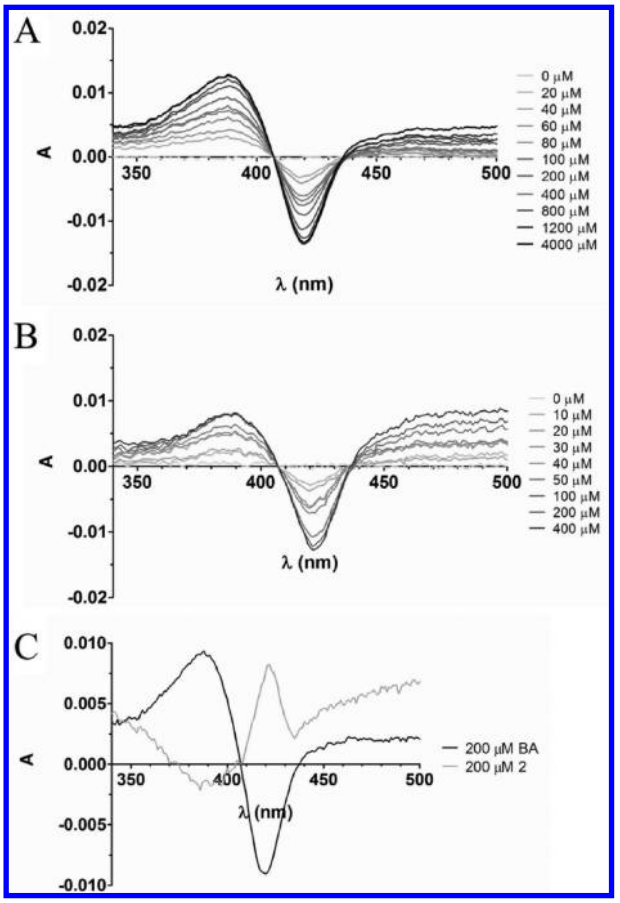

Figure 2. Difference spectra of CYP53A15, showing (A) typical substrate type I spectra upon binding of BA (0−4 mM), (B) type I spectral changes induced by interaction with compound **1** (0−0.4 mM), and (C) reverse type I spectrum produced upon binding of compound **2**.

minimum at 419 nm, and isosbestic point at 407 nm are similar to BA-induced difference spectra obtained with benzoate 4-monooxygenase from the basidiomycetous yeast *Rhodotorula minuta* having a maximum at 388 nm and a minimum at 419 nm.[38]

The majority of VS hit compounds gave rise to type I binding spectra as exemplified by compound **1** (Figure 2B). The only exception to the rule was compound **2** that produced reverse type I binding spectrum (Figure 2C) with a maximum at 422

dx.doi.org/10.1021/ci3004418 | J. Chem. Inf. Model. 2012, 52, 3053−3063

Table 1. Spectral Binding Parameters (K_s and ΔA_{max} Values) and the Magnitude of Spectral Binding ($\Delta A_{max}/K_s$) of Hit Compounds with CYP53A15

rank[a]	ID	λ_{max} (nm)	λ_{min} (nm)	ΔA_{max}	K_s (μM)	$\Delta A_{max}/K_s$
	BA	386	419	0.0155 ± 0.0026	88 ± 14	**1.76 × 10^{-4}**
I	**2**	422	386	0.0089 ± 0.0013	8.2 ± 4.6	**1.09 × 10^{-3}**
II	**10**	382	416	0.0151 ± 0.0028	36.2 ± 15.9	**4.17 × 10^{-4}**
	1	388	422	0.0114 ± 0.0023	33.3 ± 12.1	**3.42 × 10^{-4}**
	11	392	428	0.0149 ± 0.0033	44.9 ± 8.4	**3.32 × 10^{-4}**
	12	392	423	0.0195 ± 0.0045	68.6 ± 11.7	**2.84 × 10^{-4}**
III	**15**	386	419	0.0094 ± 0.0014	48.0 ± 18.6	**1.95 × 10^{-4}**
	14	381	417	0.0095 ± 0.0018	52.7 ± 27.4	**1.80 × 10^{-4}**
	13	386	417	0.0107 ± 0.0020	63.4 ± 41.6	**1.68 × 10^{-4}**
IV	**16**	383	419	0.0107 ± 0.0024	75.5 ± 21.3	**1.41 × 10^{-4}**
	17	383	417	0.0097 ± 0.0022	76.5 ± 21.7	**1.27 × 10^{-4}**
	18	383	418	0.0097 ± 0.0022	82.1 ± 31.4	**1.18 × 10^{-4}**
	19	383	418	0.0124 ± 0.0029	121.0 ± 47.2	**1.02 × 10^{-4}**
	20	386	420	0.0110 ± 0.0007	118.8 ± 25.8	**9.26 × 10^{-5}**
	21	383	420	0.0089 ± 0.0020	92.5 ± 38.0	**9.62 × 10^{-5}**
	22	385	417	0.0086 ± 0.0019	111.1 ± 51.7	**7.74 × 10^{-5}**
	6	380	421	0.0124 ± 0.0029	244.9 ± 246.3	**5.06 × 10^{-5}**
	4	383	419	0.0105 ± 0.0024	210 ± 185	**5.00 × 10^{-5}**

[a]The magnitude of spectral binding: (I) strongest; (IV) weakest.

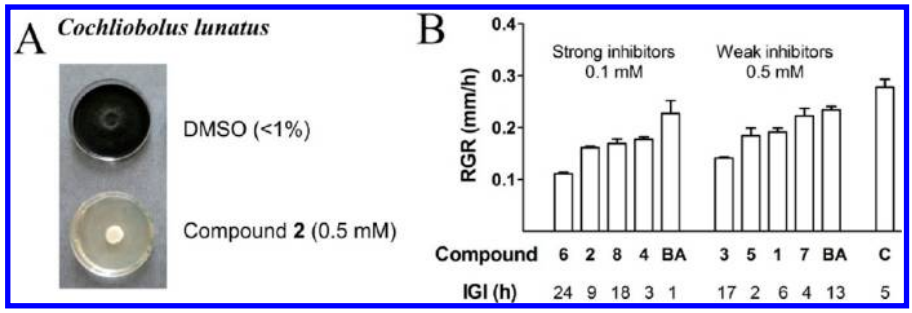

Figure 3. (A) Example of *Cochliobolus lunatus* growth inhibition by compound **2** compared to control (5 days after inoculum). (B) Radial growth rate (RGR) and initial growth inhibition (IGI) of *C. lunatus* on MEA medium supplemented with inhibitors, BA and solvent control (C; DMSO).

nm, minimum at 386 nm, and isosbestic point at 407 nm. Ligands that induce reverse type I (modified type II) spectra with CYP enzymes are characterized by formation of a peak at about 420 nm and a trough at about 392 nm in the difference spectrum, reflecting a transition from the high- to low-spin iron form.[39−41] Initially it was suggested that reverse type I spectra arise from coordination of the ligand hydroxyl group to the heme iron.[39,42,43] However, compounds without hydroxyl groups also elicit reverse type I spectra upon binding to CYPs, probably due to the alteration of the CYP active site, which mediates the entering of a water molecule as the distal ligand.[41] Water molecule-mediated binding to the heme iron upon binding of the inhibitor was also reported for the P450cam-2-phenylimidazole and CYP121-fluconazole complexes.[44,45] Reverse type I spectra were likewise recorded during the interaction of CYP125A1 and LP10,[46] a potent type II inhibitor of *Trypanosoma cruzi* CYP51.[47,48] Both the crystal structure and spectral characteristics of the CYP125A1-LP10 complex demonstrated stabilization of axial water by the incoming inhibitor and a complete shift of the heme iron spin equilibrium to the hexa-coordinated low-spin state.

Twelve compounds (**7**, **23**, **24**, **32**−**40**; Chart S1, Supporting Information) did not induce significant spectral changes, or the spectral interaction with CYP53A15 was not detectable, even at ligand concentrations as high as 200 μM. Compounds **3**, **5**, **8**, and **9** had significant absorbance in the near UV region (in absolute and difference spectra, not shown) that hindered further analysis of spectral interaction with CYP53A15.

During molecular docking, only solutions predicting interactions with the heme iron were allowed. Nevertheless, a high number of hit compounds yielding spectral interaction with CYP53A15 (more than 50% hit rate) was a pleasant surprise, and a sign that the active cavity architecture was accurately predicted by the homology model.

We calculated the spectral binding parameters (K_s and ΔA_{max} values) and magnitude of spectral binding ($\Delta A_{max}/K_s$) describing the affinity and potency of interactions between CYP53A15 and hit compounds from ligand titration curves (Table 1). We used BA as the reference. The estimated spectral dissociation constant for binding of BA to CYP53A15 (K_s = 88 μM) was approximately twice lower than K_s (36 μM) reported for benzoate 4-monooxygenase from *Rhodotorula minuta*.[38] Compound **2** had the highest magnitude of spectral binding ($\Delta A_{max}/K_s$ = 1.09 × 10^{-3}) and the strongest binding affinity with a K_s of 8.2 μM. The magnitude of spectral binding increased 1.5−2 times for compounds **1** and **10**−**12**, compared to BA ($\Delta A_{max}/K_s$ = 1.76 × 10^{-4}). The binding magnitude of compounds **13**−**15** was similar to that of BA, while the rest of the compounds (9 compounds) were bound weaker than BA.

dx.doi.org/10.1021/ci3004418 | J. Chem. Inf. Model. 2012, 52, 3053−3063

Antifungal Activity of Selected Hit Compounds. We examined a total of 33 DMSO-soluble compounds for their ability to inhibit the growth of the filamentous fungus *Cochliobolus lunatus*. As seen from Figure 3A, compound **2** completely inhibited fungal growth at 0.5 mM concentration (even after 14 days, not shown). In Figure 3B, we compared the radial growth rate (RGR; mm/h) influenced by eight active antifungal compounds (divided into two groups according to their potency) to the equivalent concentration of BA. Compound **6** was the best inhibitor of fungal growth, followed by **2**, **8**, and **4**. Compounds **3**, **5**, **1**, and **7** were weaker inhibitors of *C. lunatus*. For biochemical evaluation with CYP53A15, we selected only the compounds with antifungal activity.

Hydroxylation of BA by CYP53A15 and Inhibition Assay. We determined the catalytic properties of CYP53A15 in the reconstitution system (RS) with endogenous cytochrome P450 reductase (CPR). Using HPLC, we followed BA hydroxylation to 4-hydroxybenzoic acid in the absence and presence of putative inhibitors at different incubation times. Figure 4A displays typical progress curves in the absence of inhibitor. A double character of all curves is obvious from this diagram, differing only in the starting concentrations of the enzymes and reactants. We observed the same pattern also for the curves in the presence of eight active antifungal substances from VS. In Figure 4B, we only show the progress curves obtained at different concentrations of the most potent compound **2**.

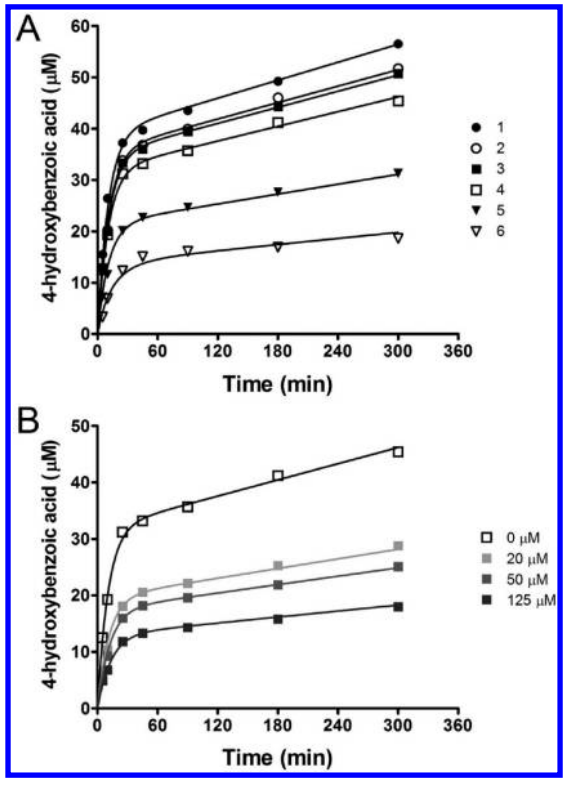

Figure 4. (A) Time course of 4-hydroxybenzoic acid formation in the reconstitution system with BA. The concentrations of BA and CYP53A15 enzyme, respectively, were: 1−118 μM, 1.1 μM; 2−93 μM, 1.0 μM; 3−120 μM, 1.1 μM; 4−57 μM, 0.7 μM; 5−27.5 μM, 0.4 μM; 6−102 μM, 1.0 μM. (B) Inhibition of CYP53A15 enzyme activity by compound **2**. Note that the curve without compound **2** is curve 4 from panel A. The concentrations of BA and CYP53A15 enzyme in all curves were 57 and 0.7 μM, respectively.

In our previous studies[19] using commercial rabbit liver CPR and DLPC vesicles, we did not observe such a double character of progress curves. We only detected the slowly increasing second part. Therefore, we searched for an appropriate mechanistic interpretation of the biphasic progress curves. Among several tested kinetic models, the one proposed in Scheme 2 best described the experimental progress curves for hydroxylation of BA by RS in the absence and presence of inhibitors.

Scheme 2. Reaction Model of BA Hydroxylation by CYP53A15 in the Absence and Presence of Inhibitors[a]

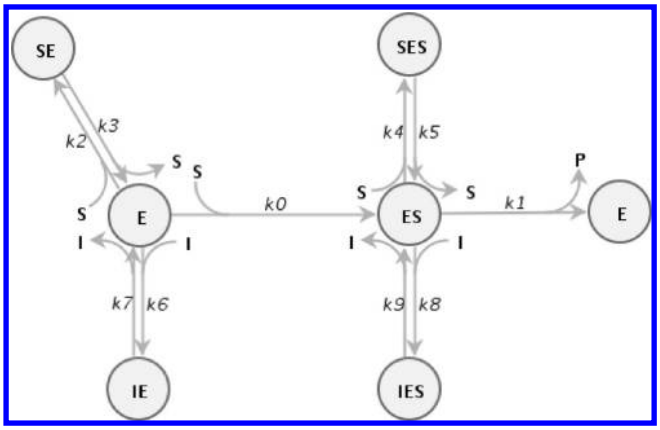

[a](S) substrate (BA); (E) enzyme (CYP53A15; benzoate 4-monooxygenase); (I) inhibitor (hit compound); (P) product (4-hydroxybenzoic acid). The letter S on the right of E represents the productive enzyme−substrate complex, while S or I on the left represent a nonproductive complex.

Besides the classical Michaelis−Menten reaction mechanism, as suggested by Van Slyke and Cullen,[49] Scheme 2 represents two additional phenomena: nonproductive binding of the substrate to the free CYP53A15 (k_3/k_2) and the inhibition by the excess of substrate (k_5/k_4). Consequently, the inhibition by hit compounds originates from their competition with the substrate for free enzyme (k_7/k_6) and the enzyme−substrate complex (k_9/k_8).

According to Scheme 2, we evaluated the characteristic kinetic constants for BA hydroxylation by CYP53A15 and the inhibition by eight putative inhibitors (Figure 5) by submitting the corresponding experimental progress curves to the ENZO web application.[27] We performed an initial analysis in two steps. In the first step, we analyzed the curves without inhibitors to determine classical kinetic parameters K_M and k_{cat}, as well as the constants concerning nonproductive binding and substrate inhibition. Since we interpreted the data in accordance with the Van Slyke−Cullen assumption, we obtained the value of K_M as a ratio between the catalytic constant (k_{cat}, k_1 in Scheme 2) and the specificity constant (k_0 in Scheme 2). The determined values for k_0 and k_1 were $1.6 \pm 0.5 \times 10^5$ M^{-1} s^{-1} and 6.8 ± 4.7 min^{-1}, respectively, yielding K_M of 42.4 μM. This value is approximately 10 times lower than previously reported K_M for BA 4-hydroxylation in reconstitution system with mammalian NADPH cytochrome P450 reductase[19] indicating the importance of the endogenous redox partner. It is also two times lower than the kinetic constant ($K_M = 83 \pm 9$ μM) calculated for BA conversion to 4-hydroxylated form by BPH in

dx.doi.org/10.1021/ci3004418 | J. Chem. Inf. Model. 2012, 52, 3053−3063

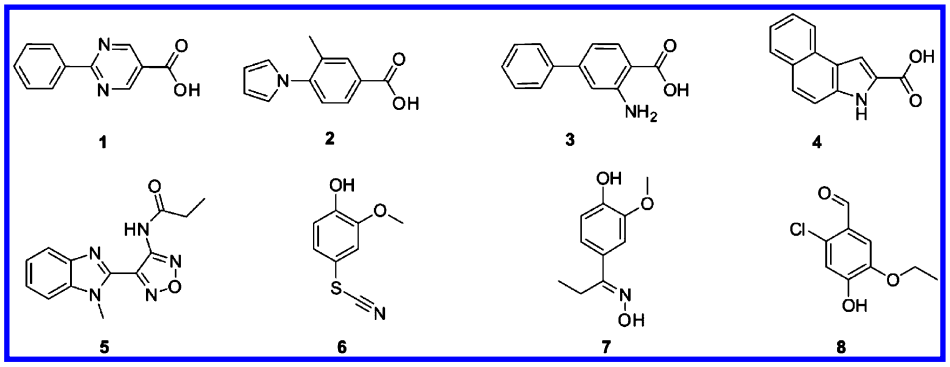

Figure 5. Structures of the best CYP53A15 inhibitors with antifungal activity.

microsomal fractions of *Aspergillus niger*.[50] On the other hand, nonproductive binding of BA occurred rarely $k_{on} = 4.8 \pm 2.4 \times 10^3$ M^{-1} s^{-1}, with high affinity (0.3 μM) and was reflected as a slowly decreasing enzyme activity. Additionally, due to the relatively long active site channel in CYP53A15 (Figure 7), the second substrate molecule, or one of a similar size and shape, can enter before the turnover of the first substrate is completed. Indeed, the orientation of the latter is kinetically irrelevant, since it always leads to the enzyme blockade. The binding of second molecule was fast, but with substantially lower affinity (126 μM).

In the second step, we determined the inhibition constants for each selected compound from the corresponding progress curves, setting the values of k_0–k_5 as fixed parameters. In the case of compound **2**, we repeated the evaluation without constraints (project ID 120402501 in ENZO application; http://enzo.cmm.ki.si/kinetic.php?uwd=120402501&load=true). The computed inhibition constants for all eight antifungal compounds are summarized in Table 2.

Table 2. Competitive and Uncompetitive Inhibition Constants for Hit Compounds That Also Exhibited Antifungal Activity

compound	K_{icomp} (μM)[a]	$K_{iuncomp}$ (μM)[b]
2	1.17	54.40
1	1.81	41.91
8	1.89	5919.20
3	4.98	56.12
7	5.52	48.95
5	9.35	38.56
4	17.55	2349.30
6	26.14	40.54

[a] $K_{icomp} = k_7/k_6$. [b] $K_{iuncomp} = k_9/k_8$.

We calculated the values of dissociation constants in the Table 2 as quotients (k_{off}/k_{on}). Since we set the k_{on} values to the constant value characteristic for diffusion (equilibrium treatment), we evaluated only standard errors for k_{off}'s. They were always less than 10%.

Structure–Activity Relationship Analysis of Hit Compounds. To identify critical structural features of eight active hit compounds, we summarized the results of spectral binding experiments, in vitro, and growth inhibition assays. The most active class were derivatives of para-substituted benzoic acid (compounds **1**, **2**, **3**), all identified by structure-based virtual screening. Members of this class share a similar structure motif: an aromatic carboxylic acid substituted at the para position with another aromatic ring. The best inhibitor was compound **2** (3-methyl-4-(1*H*-pyrrol-1-yl)benzoic acid), with a K_i value of 1.17 μM. Compound **2** was also the best in the spectral binding assay and had second best antifungal activity. Compound **1** (2-phenylpyrimidine-5-carboxylic acid) had only a slightly lower activity compared to compound **2**, with K_i value of 1.81 μM, and was also ranked high in the spectral binding assay, but surprisingly had a weak antifungal activity. This indicates that benzoic acid can be replaced by pyrimidine-5-carboxylic acid and pyrrole with phenyl, while retaining similar activity in the inhibition assay and the spectral binding assay. This change, however, had a negative impact on antifungal activity. The last member of para-substituted benzoic acid derivatives, compound **3**, had a lower activity with K_i value of 4.98 μM and had weak antifungal activity. Results of spectral binding assay were inconclusive due to absorbance of the compound in the near UV region.

Compound **4** (3*H*-benzo[e]indole-2-carboxylic acid) could also be considered chemically similar to para-substituted benzoic acid derivatives, since it is an aromatic carboxylic acid. In addition, it was identified with structure-based virtual screening; it had a K_i value of 17.55 μM and induced a weak response in the spectral binding assay. Interestingly, it had good antifungal activity.

Compounds **6**, **7**, and **8** can also be grouped in the same chemical class. They are all catechol derivatives and were identified with ligand-based screening, where isoeugenol was used as a query. This group of compounds has one free OH group and the other either methylated or ethylated, and different substituents on para position relative to the free OH group. Compound **8** (2-chloro-5-ethoxy-4-hydroxybenzaldehyde) exhibited the best inhibitory activity of this series with K_i value of 1.89 μM, and it also had good antifungal activity. Results of the spectral binding assay were inconclusive due to absorbance of the compound in the near UV region. Compound **8** is closely followed by compound **7** ((*E*)-1-(4-hydroxy-3-methoxyphenyl)propan-1-one oxime) with K_i value of 5.52 μM and weak antifungal activity. Interestingly, it did not induce significant spectral changes, indicating that interaction of compound **7** with the heme iron is very weak. The last compound in this class is compound **6** (2-methoxy-4-thiocyanatophenol) with a K_i value of 26.14 μM and a minor spectral change in spectral binding assay. Surprisingly, this compound had the best antifungal activity of inhibitors reported in this study.

Compound **5** (*N*-(4-(1-methyl-1*H*-benzo[d]imidazol-2-yl)-1,2,5-oxadiazol-3-yl)propionamide) cannot be grouped in either of the above classes. It was identified by structure-

dx.doi.org/10.1021/ci3004418 | J. Chem. Inf. Model. 2012, 52, 3053–3063

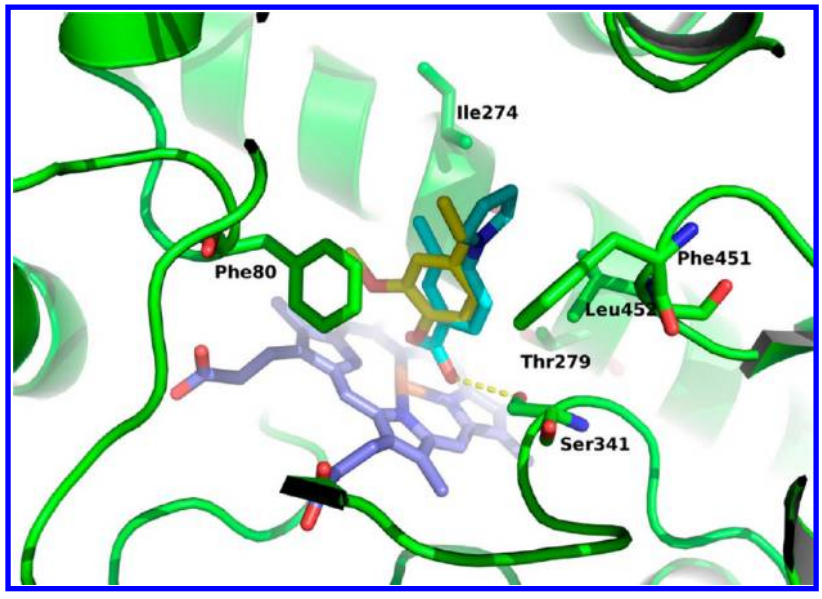

Figure 6. Docking of compound **2** (cyan) versus the conformation of isoeugenol (yellow) in the active site of the homology-built model of CYP53A15 (green ribbon).[19]

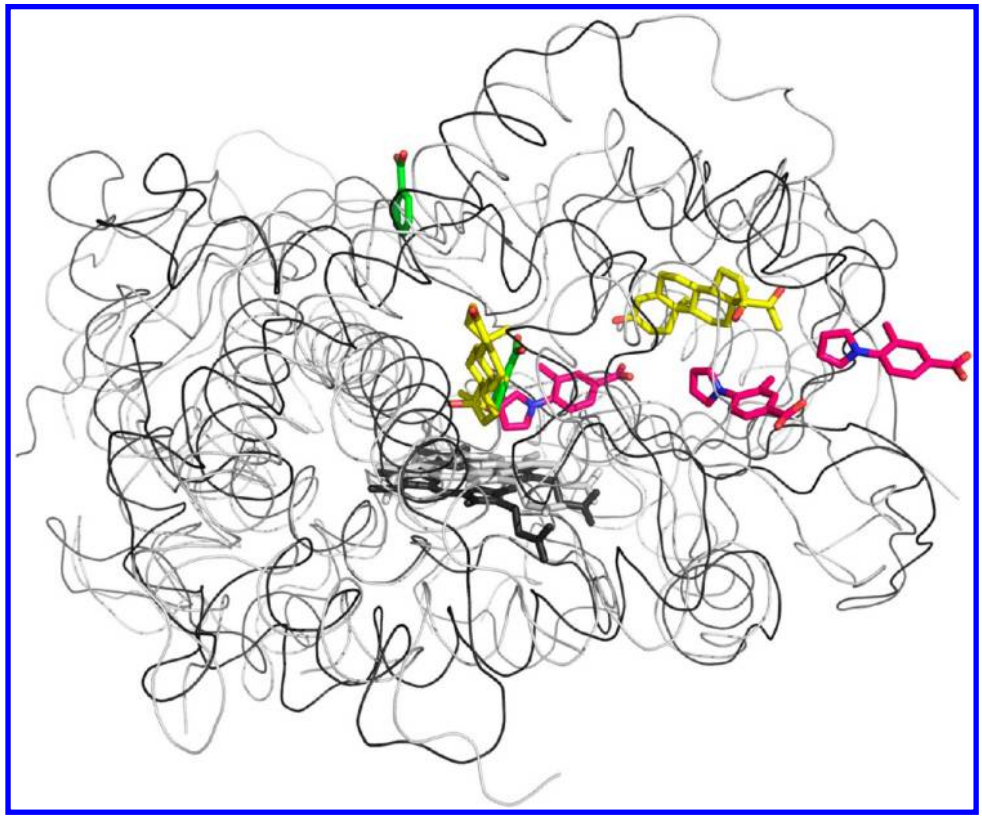

Figure 7. CYP53A15 homology model (in dark gray) superimposed with crystal structure of bovine CYP21A1 (light gray) complexed with substrate ((9β)-17-hydroxypregn-4-ene-3,20-dione; yellow). Note the simultaneous binding of substrate (BA; green) above the heme and inhibitor (compound **2**; magenta) entering the CYP53A15 active site channel.

based virtual screening and has a K_i value of 9.35 μM and weak antifungal activity. Recording spectral changes in the spectral binding assay was hindered, because this compounds absorbs in the near UV region.

Overall, potent inhibitors of CYP53A15 were identified with structure-based virtual screening. Structure-based virtual screening also yielded more diverse compounds. On the other hand, the compound with the best antifungal activity was identified with ligand-based virtual screening. Both methods gave satisfactory results and had high hit rates. This indicates that they should be used complementarily, each identifying compounds from different regions of chemical space.

Molecular Docking and Molecular 3D Simulation of CYP53A15 Inhibition. VS generated hydrophobic hit compounds. As illustrated by compound **2** (Figure 6), their predicted binding mode obtained by FlexX[22] matches that of

dx.doi.org/10.1021/ci3004418 | J. Chem. Inf. Model. 2012, 52, 3053−3063

isoeugenol in the CYP53A15 active site of the homology model.[19] The π-stacking interactions between Phe80 and the aromatic ring of compound **2**, as well as between Phe451 (which lies perpendicular to Phe80) and a pyrrole ring of compound **2** are critical in the positioning of the ligand. Anchoring is further stabilized by favorable hydrophobic interactions with Ile274 and Leu452. Close proximity of Ser341 to the carboxy group of compound **2** allows possible H-bonding and may contribute to ligand recognition.

The kinetic interpretation of CYP53A15 inhibition by hit compounds agrees with the reaction mechanism predicted in Scheme 2. It assumes that CYP53A15 is membrane-bound and suggests that the hydrophobic ligands enter the active site (characteristic constant K_{icomp}) through a channel, that is surrounded by numerous nonpolar residues including four prolines (characteristic constant $K_{iuncomp}$) and is adjacent to the membrane-anchoring N-terminus. This reasoning is summarized in the 3D molecular simulation of the path of compound **2** through the active channel of CYP53A15 (see movie in the Supporting Information). Figure 7 displays CYP53A15 (dark gray backbone) with three particular positions of the inhibitor (stick structures in magenta), from the entrance toward its arrangement above the heme.

The depicted interpretation is based on structural and chemical characteristics of the enzyme, substrate, and all tested inhibitors, and strongly agrees with the observed overall kinetics. Indeed, extensive molecular 3D simulations together with free-energy calculations might provide further details of studied interactions.[51] However, our intention was solely to visualize kinetic findings in the form of 3D complexes of CYP53A15 with substrate and best hit ligand considering stearic requirements of the active site. Finally, it seems that multiple ligand binding into the channel is a more general feature of CYP enzymes.[51,52] Recently, crystallographic evidence showed two steroid substrate molecules resolved in the channel of another CYP.[53] Therefore, in Figure 7, we superimposed the structure deposited in PDB under code no. 3QZ1 over our homology model. Interestingly, the unexpected orientation of the two (9β)-17-hydroxypregn-4-ene-3,20-dione molecules (colored yellow in Figure 7) inside the active site of bovine P450C21 (CYP21A1) corroborates the interpretation of nonproductive binding mechanism in our CYP53A15.

CONCLUSIONS

In this work, we have demonstrated the utility of two parallel VS approaches, a ligand-based similarity search and a model/structure-based VS, to narrow down the selection of possible CYP53A15 substrates and inhibitors for further experimental verification. Through an in vitro approach where we performed spectral binding titrations with CYP53A15, we validated the hit compounds as ligands. Interestingly, over 50% of tested compounds formed interactions with heme iron. Further, we established their antifungal potential through in vivo fungal growth experiments and confirmed four potent (compounds **2**, **4**, **6**, and **8**) and four weaker (**1**, **3**, **5**, and **7**) inhibitors. When we analyzed the eight compounds in enzymatic tests with CYP53A15 using HPLC, we found that compounds **1**, **2**, and **8** were the most effective inhibitors.

In conclusion, we have shown that our dual VS approach effectively produced a manageable selection of potential antifungals and that our complementary approach to experimentally validating inhibitory compounds further narrowed down the list of best inhibitors. Compound **2** is a good inhibitor of a fungal-specific enzyme, and a promising new hit compound in an antifungal market where novel drug targets and good inhibitors are scarce.

ASSOCIATED CONTENT

Supporting Information

Figure S1: Protein alignment of selected fungal CYP53 members and characteristic structural features.

Chart S1: Structures, FlexX, Ftrees scores, and ranks of 40 hit compounds from virtual screening.

Table S1: Compound 2 chemical scheme, CHARMM atom names, types and partial atomic charges, and applied bonding parameters.

Chemical characterization: HPLC purity, ^{1}H NMR, and MS spectral data of active hit compounds from virtual screening.

Visualization of the 3D molecular simulation: Path of compound **2** through the active channel of CYP53A15.

This material is available free of charge via the Internet at http://pubs.acs.org.

AUTHOR INFORMATION

Corresponding Author

*E-mail: sabina.berne@mf.uni-lj.si. Telephone: +386-1-5437644. Fax: +386-1-5437641 (S.B.). E-mail: radovan.komel@ki.si. Telephone: +386-1-4760465. Fax: +386-1-4760300 (R.K.).

Author Contributions

$^{\|}$These authors contributed equally.

Notes

The authors declare no competing financial interest.

ACKNOWLEDGMENTS

We thank OpenEye Scientific Software, Inc. for free academic licenses of their software. The financial support from Slovenian Research Agency by Grants J4-2212 and P1-0104 is gratefully acknowledged. We would also like to thank John D. Crolla for critical reading of the manuscript.

ABBREVIATIONS

BA, benzoic acid; CYP, cytochrome P450; CPR, cytochrom P450 reductase; RS, reconstitution system; VS, virtual screening

REFERENCES

(1) Pfaller, M. A.; Diekema, D. J. Epidemiology of invasive mycoses in North America. *Crit. Rev. Microbiol.* **2010**, *36*, 1−53.

(2) Owens, J. N.; Skelley, J. W.; Kyle, J. A. The fungus among us: an antifungal review. *US Pharm.* **2010**, *35* (8), 44−56.

(3) Low, C.-Y.; Rotstein, C. Emerging fungal infections in immunocompromised patients. *F1000 Med. Rep.* **2011**, *3*, 14.

(4) Miceli, M. H.; Lee, S. Emerging moulds: epidemiological trends and antifungal resistance. *Mycoses [Online]* **2011**, *54*, e666−678.

(5) Perfect, J. R. Azoles: back to the future. *Curr. Opin. Infect. Dis.* **2011**, *24*, S41−S58.

(6) Eschenauer, G.; Depestel, D. D.; Carver, P. L. Comparison of echinocandin antifungals. *Ther. Clin. Risk Manag.* **2007**, *3*, 71−97.

(7) *Antifungals market to 2017 - Generic erosion of major polyenes, azoles, allylamines and echinocandins to slow value growth*; GBI Research report, Jan 2012; 118 pp, report code: ASDR-25413; http://www.docstoc.com/docs/110983114/Antifungals-Market-to-2017---Generic-Erosion-of-Major-Polyenes-Azoles-Allylamines-and-Echinocandins-to-Slow-Value-Growth (accessed May 9, 2012).

(8) Chen, S. C.-A; Playford, E. G.; Sorrell, T. C. Antifungal therapy in invasive fungal infections. *Curr. Opin. Pharmacol.* **2010**, *10*, 522−530.

(9) Ostrosky-Zeichner, L.; Casadevall, A.; Galgiani, J. N.; Odds, F. C.; Rex, J. H. An insight into the antifungal pipeline: Selected new molecules and beyond. *Nat. Rev. Drug Disc.* **2010**, *9*, 719−727.
(10) Johnson, M. D.; Perfect, J. R. Use of Antifungal combination therapy: agents, order, and timing. *Curr. Fungal Inf. Rep.* **2010**, *4*, 87−95.
(11) Gubbins, P. O. Triazole antifungal agents drug−drug interactions involving hepatic cytochrome P450. *Exp. Opin. Drug Metabol. Toxicol.* **2011**, *7*, 1411−1429.
(12) Denning, D. Antifungals: Where are we headed? *Drug Plus Internat.* [Online] (Sept. 21 **2004**); http://pharmalicensing.com/public/articles/view/1095693369_414ef439d6909 (accessed May 9, 2012).
(13) Maertens, J. A. History of the development of azole derivatives. *Clin. Microbiol. Infect.* **2004**, *10*, 1−10.
(14) Guengerich, F. P.; Wu, Z.-L.; Bartleson, C. J. Function of human cytochrome P450s: characterization of the orphans. *Biochem. Biophys. Res. Commun.* **2005**, *338*, 465−469.
(15) Kashuba, A. D. M.; Bertino, J. S. J. Mechanisms of drug interactions I. Absorption, Metabolism, and Excretion. In *Drug Interactions in Infectious Diseases*, 2nd ed.; Piscitelli, S. C., Rodvold, K. A., Eds.; Humana Press: Totowa, NJ, 2005; pp 13−39.
(16) Schuster, I.; Bernhardt, R. Inhibition of Cytochromes P450: Existing and new promising therapeutic targets. *Drug Metabol. Rev.* **2007**, *39* (2−3), 481−499.
(17) Sheehan, D. J.; Hitchcock, C. A.; Sibley, C. M. Current and emerging azole antifungal agents. *Clin. Microbiol. Rev.* **1999**, *12*, 40−79.
(18) Ashkenazy, H.; Erez, E.; Martz, E.; Pupko, T.; Ben-Tal, N. ConSurf 2010: calculating evolutionary conservation in sequence and structure of proteins and nucleic acids. *Nucleic Acids Res.* **2010**, *38*, W529-533.
(19) Podobnik, B.; Stojan, J.; Lah, L.; Kraševec, N.; Seliškar, M.; Rižner, T. L.; Rozman, D.; Komel, R. CYP53A15 of *Cochliobolus lunatus*, a Target for Natural Antifungal Compounds. *J. Med. Chem.* **2008**, *51*, 3480−3486.
(20) Irwin, J. J.; Shoichet, B. K. ZINC: A free database of commercially available compounds for virtual screening. *J. Chem. Info. Model* **2005**, *45*, 177−182.
(21) Shoichet, B. K. Interpreting steep dose response curves in early inhibitor discovery. *J. Med. Chem.* **2006**, *49*, 7274−7277.
(22) Rarey, M.; Kramer, B.; Lengauer, T.; Klebe, G. A fast flexible docking method using an incremental construction algorithm. *J. Mol. Biol.* **1996**, *261*, 470−489.
(23) Rarey, M.; Dixon, J. S. Feature trees: A new molecular similarity measure based on tree matching. *J. Comput. Aided Mol. Des.* **1998**, *12*, 471−490.
(24) Lah, L.; Kraševec, N.; Trontelj, P.; Komel, R. High diversity and complex evolution of fungal cytochrome P450 reductase: cytochrome P450 systems. *Fungal Genet. Biol.* **2008**, *45* (4), 446−458.
(25) Bradford, M. M. A rapid and sensitive method for the quantitation of microgram quantities of protein utilizing the principle of protein-dye binding. *Anal. Biochem.* **1976**, *72*, 248−254.
(26) Jefcoate, C. R. Measurement of substrate and inhibitor binding in microsomal cytochrome-P450 by optical-difference spectroscopy. In *Methods in Enzymology*; Fleischer, S., Packer, L., Eds.; Academic Press: New York, 1978; Vol. *52*, pp 258−279.
(27) Bevc, S.; Konc, J.; Stojan, J.; Hodošček, M.; Penca, M.; Praprotnik, M.; Janežič, D. ENZO: a Web Tool for Derivation and Evaluation of Kinetic Models of Enzyme Catalyzed Reactions. *PLoS ONE* [Online] **2011**, *6* (7), e22265; doi:10.1371/journal.pone.0022265.
(28) Castrignanò, T.; De Meo, P. D.; Cozzetto, D.; Talamo, I. G.; Tramontano, A. The PMDB Protein Model Database. *Nucleic Acids Res.* [Online] **2006**, *34*, D306−D309; doi:10.1093/nar/gkj105.
(29) Brooks, B. R.; Bruccoleri, R. E.; Olafson, B. D.; States, D. J.; Swaminathan, S.; Karplus, M. CHARMM: A program for macromolecular energy, minimization and dynamics calculation. *J. Comput. Chem.* **1983**, *4*, 187−217.
(30) Humphrey, W.; Dalke, A.; Schulten, K. VMD: Visual Molecular Dynamics. *J. Mol. Graph.* **1996**, *14*, 33−38.
(31) Shoichet, B. K. Virtual screening of chemical libraries. *Nature* **2004**, *432*, 862−865.
(32) Reddy, A. S.; Pati, S. P.; Kumar, P. P.; Pradeep, H. N.; Sastry, G. N. Virtual screening in drug discovery - a computational perspective. *Curr. Prot. Pept. Sci.* **2007**, *8*, 329−351.
(33) Schneider, G. Virtual screening: an endless staircase? *Nat. Rev. Drug Disc.* **2010**, *9*, 273−276.
(34) Carr, R. A. E.; Congreve, M.; Murray, C. W.; Rees, D. C. Fragment-based lead discovery: leads by design. *Drug Discov. Today* **2005**, *10* (14), 987−992.
(35) Ripphausen, P.; Nisius, B.; Peltason, L.; Bajorath, J. Quo vadis, virtual screening? A comprehensive survey of prospective applications. *J. Med. Chem.* **2010**, *53* (24), 8461−8467.
(36) Schenkman, J. B.; Remmer, H.; Estabrook, R. W. Spectral studies of drug interaction with hepatic microsomal cytochrome. *Mol. Pharmacol.* **1967**, *3*, 113−123.
(37) Schenkman, J. B.; Sligar, S. G.; Cinti, D. L. Substrate interaction with cytochrome P-450. *Pharmacol. Therapeut.* **1981**, *12* (1), 43−71.
(38) Fukuda, H.; Nakamura, K.; Sukita, E.; Ogawa, T.; Fujii, T. Cytochrome P450rm from *Rhodotorula minuta* catalyzes 4-hydroxylation of benzoate. *J. Biochem.* **1996**, *119*, 314−318.
(39) Schenkman, J. B.; Cinti, D. L.; Orrenius, S.; Moldeus, P.; Kraschnitz, R. The nature of the reverse type I (modified type II) spectral change in liver microsomes. *Biochemistry* **1972**, *11* (23), 4243−4251.
(40) Wilson, B. J.; Orrenius, S. A study of the modified type II spectral change produced by the interaction of agroclavine with cytochrome P-450. *Biochim. Biophys. Acta* **1972**, *261*, 94−101.
(41) Shimada, T.; Tanaka, K.; Takenaka, S.; Foroozesh, M. K.; Murayama, N.; Yamazaki, H.; Guengerich, F. P.; Komori, M. Reverse type I binding spectra of human cytochrome P450 1B1 induced by flavonoid, stilbene, pyrene, naphthalene, phenanthrene, and biphenyl derivatives that inhibit catalytic activity: a structure-function relationship study. *Chem. Res. Toxicol.* **2009**, *22*, 1325−1333.
(42) Yoshida, Y.; Kumaoka, H. Studies on the substrate-induced spectral change of cytochrome P-450 in liver microsomes. *J. Biochem.* **1975**, *78*, 55−68.
(43) Kumaki, K.; Sato, M.; Kon, H.; Nebert, D. W. Correlation of type I, type II, and reverse type I difference spectra with absolute changes in spin state of hepatic microsomal cytochrome P-450 iron from five mammalian species. *J. Biol. Chem.* **1978**, *253*, 1048−1058.
(44) Poulos, T. L.; Howard, A. J. Crystal structures of metyrapone- and phenylimidazole-inhibited complexes of cytochrome P-450cam. *Biochemistry* **1987**, *26*, 8165−8174.
(45) Seward, H. E.; Roujeinikova, A.; McLean, K. J.; Munro, A. W.; Leys, D. Crystal structure of the *Mycobacterium tuberculosis* P450 CYP121-fluconazole complex reveals new azole drug-P450 binding mode. *J. Biol. Chem.* **2006**, *281*, 39437−39443.
(46) Ouellet, H.; Kells, P. M.; Ortiz De Montellano, P. R.; Podust, L. M. Reverse type I inhibitor of *Mycobacterium tuberculosis* CYP125A1. *Bioorg. Med. Chem. Lett.* **2011**, *21*, 332−337.
(47) Chen, C.-K.; Doyle, P. S.; Yermalitskaya, L. V.; Mackey, Z. B.; Ang, K. K. H.; McKerrow, J. H.; Podust, L. M. *Trypanosoma cruzi* CYP51 inhibitor derived from a *Mycobacterium tuberculosis* screen hit. *PLoS Negl. Trop. Dis.* [Online] **2009**, *3* (2), e372; doi: 10.1371/journal.pntd.0000372.
(48) Doyle, P. S.; Chen, C.-K.; Johnston, J. B.; Hopkins, S. D.; Leung, S. S. F.; Jacobson, M. P.; Engel, J. C.; McKerrow, J. H.; Podust, L. M. A non-azole CYP51 inhibitor cures Chagas Disease in a mouse model of acute infection. *Antimicrob. Agents Chemother.* **2010**, *54* (6), 2480−2488.
(49) Van Slyke, D. D.; Cullen, G. E. The mode of action of urease and of enzymes in general. *J. Biol. Chem.* **1914**, *19*, 141−180.
(50) Faber, B. W.; van Gorcom, R. F.; Duine, J. A. Purification and characterization of benzoate-para-hydroxylase, a cytochrome P450 (CYP53A1), from *Aspergillus niger*. *Arch. Biochem. Biophys.* **2001**, *394* (2), 245−254.

(51) Stjernschantz, E.; Vermeulen, N. P. E.; Oostenbrink, C. Computational predicition of drug binding and rationalisation of selectivity towards cytochromes P450. *Exp. Opin. Drug Metab. Toxicol.* **2008**, *4* (5), 513−527.
(52) Bren, U.; Oostenbrink, C. Cytochrome P450 3A4 inhibition by ketoconazole: Tackling the problem of ligand cooperativity using molecualr dynamics simulations and free-energy calcualtions. *J. Chem. Inf. Model* **2012**, *52*, 1573−1582.
(53) Zhao, B.; Lei, L.; Kagawa, N.; Sundaramoorthy, M.; Banerjee, S.; Nagy, L. D.; Guengerich, F. P.; Waterman, M. R. Three-dimensional structure of steroid 21-hydroxylase (Cytochrome P450 21A2) with two substrates reveals locations of disease-associated variants. *J. Biol. Chem.* **2012**, *287* (13), 10613−10622.